

The formation history of elliptical galaxies

Gabriella De Lucia^{1*}, Volker Springel¹, Simon D. M. White¹, Darren Croton^{1†}
and Guinevere Kauffmann¹

¹*Max-Planck-Institut für Astrophysik, Karl-Schwarzschild-Str. 1, D-85748 Garching, Germany*

4 February 2008

ABSTRACT

We take advantage of the largest high-resolution simulation of cosmic structure growth ever carried out – the *Millennium Simulation* of the concordance Λ CDM cosmogony – to study how the star formation histories, ages and metallicities of elliptical galaxies depend on environment and on stellar mass. We concentrate on a galaxy formation model which is tuned to fit the joint luminosity/colour/morphology distribution of low redshift galaxies. Massive ellipticals in this model have higher metal abundances, older luminosity-weighted ages, shorter star formation timescales, but lower assembly redshifts than less massive systems. Within clusters the typical masses, ages and metal abundances of ellipticals are predicted to decrease, on average, with increasing distance from the cluster centre. We also quantify the effective number of progenitors of ellipticals as a function of present stellar mass, finding typical numbers below 2 for $M_* < 10^{11} M_\odot$, rising to ~ 5 for the most massive systems. These findings are consistent with recent observational results that suggest “down-sizing” or “anti-hierarchical” behaviour for the star formation history of the elliptical galaxy population, despite the fact that our model includes all the standard elements of hierarchical galaxy formation and is implemented on the standard, Λ CDM cosmogony.

Key words: galaxies: formation – galaxies: evolution – galaxies: elliptical and lenticular, cD – galaxies: bulges – galaxies: stellar content

1 INTRODUCTION

Elliptical galaxies are the most massive stellar systems in the local Universe and appear to define a homogeneous class of objects with uniformly old and red populations, negligible amounts of gas, and very little star formation. Their deceptively simple appearance inspired a ‘classical’ formation scenario in which they form in a single intense burst of star formation at high redshifts ($z \gtrsim 5$), followed by passive evolution of their stellar populations to the present day (Partridge & Peebles 1967; Larson 1975). This so-called *monolithic* scenario successfully explains the tightness of the fundamental scaling relations that elliptical galaxies obey, like the colour–magnitude relation and the fundamental plane, as well as the evolution of these relations as a function of redshift (Kodama et al. 1998; van Dokkum & Stanford 2003).

This classical view has been tenaciously resistant to challenges by other theoretical models, despite numerous indications for a more complex formation scenario.

Toomre & Toomre (1972) suggested that elliptical galaxies can form from major mergers of massive disk galaxies. Detailed numerical simulations (Farouki & Shapiro 1982; Negroponte & White 1983) later showed that the merger of two spiral galaxies of comparable mass can indeed produce a remnant with structural and photometric properties resembling those of elliptical galaxies. In more recent years, a large body of observational evidence has been collected that demonstrates that interactions and mergers indeed represent a common phenomenon at high redshifts, and that these processes affect the population of elliptical galaxies in the local Universe. Schweizer & Seitzer (1992) found evidence for bluer colours of elliptical galaxies with increasing morphological disturbance in a study based on a small sample with a strong bias towards isolated systems (see Michard & Prugniel 2004). Later studies using absorption–line indices have demonstrated that a significant fraction of cluster early–type galaxies has undergone recent episodes of star formation (Barger et al. 1996). Signs of recent star formation activity have also been detected in a number of high redshift early–type galaxies using colours (Menanteau, Abraham & Ellis 2001; van de Ven, van Dokkum & Franx 2003) and absorption and emission line diagnostics (Treu et al. 2002; Willis et al.

* Email: gdelucia@mpa-garching.mpg.de

† Present address: Department of Astronomy, University of California, Berkeley, CA 94720.

2002). These results favour, at least for a part of the elliptical galaxy population, a *hierarchical* formation scenario in which larger spheroidals are assembled relatively late from the merger of late-type galaxies of comparable mass. Such a bottom-up formation scenario is naturally expected for the structure formation process in cosmologies dominated by cold dark matter.

However, despite an enormous amount of work both on the theoretical and on the observational side, the debate concerning the two competing theories for the formation of elliptical galaxies has remained open. As described above, a relatively large fraction of early-type systems shows clear evidence of interactions, mergers, and recent star formation. However, the data also seem to indicate that only a small fraction of the mass is involved in such episodes. The latter observational result has often been interpreted as strong evidence against the more extended star formation history naively predicted from hierarchical models. A related issue concerns the α -element enhancements observed in ellipticals. The so-called α -elements are released mainly by supernovae type-II, while the main contribution to the Fe-peak elements comes from supernovae type-Ia. For these reasons, the $[\alpha/\text{Fe}]$ ratio is believed to encode important information on the time-scale of star formation. It is now a well established result that massive ellipticals have super-solar $[\alpha/\text{Fe}]$ ratios, suggesting that they formed on relatively short time-scales and/or have an initial mass function that is skewed towards massive stars. The inability of early models of the hierarchical merger paradigm to reproduce this observed trend has been pointed out as a serious problem for these models (Thomas 1999).

Another contentious issue is related to the significantly dissimilar evolution of early-type galaxies in different environments predicted by early semi-analytic models of galaxy formation (Kauffmann 1996b; Baugh, Cole & Frenk 1996). Such differential evolution is a natural outcome of the hierarchical scenario, because present day clusters of galaxies form from the highest peaks in the primordial density fields, leading to an earlier onset of the collapse of the dark matter haloes and to more rapid mergers (Kauffmann 1995).

In recent years, considerable observational progress has been made in the study of the stellar populations of elliptical galaxies in different environments and at different redshifts (e.g. Thomas et al. 2005; Denicoló et al. 2005; Treu et al. 2005; van der Wel et al. 2005). One has to bear in mind however that the derived ages and metallicities depend quite strongly on the models employed in the analysis, primarily because of an essentially unavoidable intrinsic age-metallicity degeneracy, which appears to be stronger for older and more metal rich systems (Denicoló et al. 2005). The situation is especially unclear for ‘field’ galaxies, since here the very definition of ‘field’ is fraught with ambiguities. Significant systematic uncertainties are also present in theoretical models used for studying galaxy formation, where poorly understood physical processes need to be treated with coarse approximations in order to predict observable properties of galaxies.

A detailed analysis of the properties of elliptical galaxies expected in the framework of hierarchical galaxy formation has been given in a number of papers (Kauffmann 1996b; Baugh et al. 1996; Kauffmann & Charlot 1998). This early work used an extension of the Press-Schechter theory to pro-

duce Monte Carlo realizations of the merger trees of dark matter haloes, thus allowing the progenitors of a dark matter halo to be followed back in time to arbitrarily high redshifts. A drawback of this approach is its lack of spatial information on the clustering of galaxies. Another lies in the inherent inaccuracies of the Press-Schechter formalism. Recent years have witnessed substantial progress in this regard with the advent of ‘hybrid’ techniques where high-resolution N-body simulations of structure formation are used to directly measure dark matter merger history trees from simulations which are then combined with semi-analytic simulations of the galaxy formation physics (Kauffmann et al. 1999; Springel et al. 2001; Mathis et al. 2002). This allows the spatial and kinematic distribution of model galaxies to be predicted as a function of redshift, providing a more direct and more powerful comparison between theoretical predictions and observational results. Also, this approach eliminates much of the uncertainty introduced by Monte-Carlo prescriptions for producing mock merging histories.

Most previous semi-analytic studies of the properties of ellipticals were carried out in the framework of a cosmological model with critical matter density. This cosmogony has been replaced in recent years by the Λ CDM scenario, which has become the *de facto* standard cosmological model, thanks to its concordance with a variety of observational data, including the most recent cosmic microwave background measurements, distant supernova observations, and cosmic shear measurements. Given that both the cosmological model and the modelling techniques have changed significantly, it is interesting to revisit the question of the formation and evolution of elliptical galaxies. In this paper, we present the results of applying a semi-analytic model that tracks dark matter halos and their embedded substructures to the largest high-resolution simulation of cosmic structure growth ever carried out. Here we concentrate on the analysis of the star formation histories, the ages, and the metallicities of model elliptical galaxies as a function of galaxy mass and of environment. In a companion paper, we will study how the distribution of metallicities and ages depends on the feedback model and on the chemical enrichment scheme employed, exploring also the relative contribution of these two in shaping observed scaling properties like the colour-magnitude relation.

The layout of this paper is as follows. In Section 2, we briefly describe the simulation used in our study, and in Section 3 we give a concise overview of the semi-analytic model employed for our analysis. In Section 4, we discuss how the star formation history of model elliptical galaxies depends on the stellar mass of galaxies and on the environment, while Section 5 discusses the dependence of ages and metallicities on galaxy mass and environment. Finally, in Section 6, we summarise and discuss our findings, and give our conclusions.

2 THE SIMULATION

In this study, we analyse a large collisionless cosmological simulation which follows $N = 2160^3$ particles of mass $8.6 \times 10^8 h^{-1} M_{\odot}$ within a comoving box of size $500 h^{-1} \text{Mpc}$ on a side (Springel et al. 2005). The spatial resolution is $5 h^{-1} \text{kpc}$, available everywhere in the periodic box. The

cosmological model is a Λ CDM model with parameters $\Omega_m = 0.25$, $\Omega_b = 0.045$, $h = 0.73$, $\Omega_\Lambda = 0.75$, $n = 1$, and $\sigma_8 = 0.9$, where the Hubble constant is parameterised as $H_0 = 100 h \text{ km s}^{-1} \text{ Mpc}^{-1}$. These cosmological parameters are consistent with recent determinations from the combined analysis of the 2dFGRS (Colless et al. 2001) and first year WMAP data (Spergel et al. 2003).

A remarkable aspect of this *Millennium Simulation* carried out by the Virgo Consortium¹ is its good mass resolution combined with a very large particle number, more than 10 billion. It is the largest high-resolution simulation of cosmic structure growth carried out so far. This provides substantial statistical power, sampling the formation history even of rare objects in a representative fashion. Gao et al. (2005) have exploited this to show that the clustering of halos of fixed mass *does depend* on their formation redshift, an effect that is weak for massive systems but becomes progressively stronger towards smaller galaxies. We note that simpler schemes for modelling the galaxy distribution, based for example on the halo occupation distribution schemes or on Monte Carlo halo merger trees, do not account for this effect, highlighting the importance of direct simulations of structure formation for obtaining fully reliable merger histories.

The simulation has sufficient resolution to track the motion of dark matter substructures in massive halos, making it possible to follow the orbits of cluster ellipticals in an unambiguous fashion. During the simulation, 64 time slices were saved, together with group catalogues and their embedded substructures, the latter defined as locally over-dense and self-bound structures, identified with the SUBFIND algorithm (Springel et al. 2001). These group catalogues were then used to construct detailed merging history trees of all gravitationally self-bound dark matter structures (Springel et al. 2005). The merger trees describe the assembly of about 20 million galaxies, and form the basic input needed by the semi-analytic simulation of the galaxy formation process considered in this study.

3 THE SEMI-ANALYTIC MODEL

Our technique for grafting the semi-analytic model onto the Millennium Simulation is similar in spirit to that used by Springel et al. (2001) and De Lucia, Kauffmann & White (2004), but has been updated in a number of important points. A full description of the model is given by Springel et al. (2005) and Croton et al. (2005), but we here give a brief account of those aspects that are particularly relevant for the present study.

One of the key differences of our approach from traditional semi-analytic models is that we explicitly follow dark matter haloes even after they are accreted onto larger systems. This allows the dynamics of satellite galaxies residing in the infalling haloes to be properly followed until the parent dark matter ‘substructure’ is completely destroyed because of tidal truncation and stripping (De Lucia et al.

2004a; Gao et al. 2004). At this point, we estimate a residual survival time of the satellite galaxy and track its position by means of the most bound particle of the subhalo identified just before the substructure was disrupted. In this work, we consider as genuine substructures those subhalos that contain at least 20 self-bound particles. The parent catalogue of dark matter haloes, which are analysed for substructures and decomposed accordingly, is identified with a standard friends-of-friends (FOF) algorithm with a linking length of 0.2 in units of the mean particle separation. In our model, we assume that only the galaxy located at the position of the most bound particle of the FOF halo - the ‘central galaxy’ - is fed by radiative cooling from the surrounding halo, i.e. genuine satellite galaxies cannot replenish their reservoir of cold gas. Gas infall and cooling are modelled as described in detail in Croton et al. (2005).

Hierarchical merging trees form the backbone of our semi-analytic model, and are built for all the self-bound dark matter haloes and subhalos in the Millennium Simulation using the methods described in Springel et al. (2005): the descendant in the next time slice of each dark matter (sub)halo is identified as the (sub)halo that contains the largest number of its most tightly bound particles. Individual trees are stored separately in a self-contained fashion, so that the semi-analytic code can be run for each of these trees sequentially, instead of having to process the whole galaxy population in one single run for the entire simulation box. This makes the computation feasible even on small workstations and allows for easy parallelisation, such that the computation of the galaxy properties can be repeated with different physical assumptions in a matter of hours, if desired.

The descriptions we adopted for modelling the various mixing and exchange processes occurring between different galactic phases (stars and cold gas, hot diffuse gas in the dark matter haloes, and intergalactic gas outside virialized haloes) are essentially the same as those in De Lucia et al. (2004b). In the present study, we use their ‘ejection slow’ feedback model, which has been shown to reproduce both the observed relation between stellar mass and cold phase metallicity, and the relation between luminosity and cold gas fraction for galaxies in the local Universe, as well as the observed decline in baryon fraction from rich clusters to galaxy groups. As in De Lucia et al. (2004b), we use metallicity-dependent cooling rates and luminosities, and we refer the reader to the original paper for more details on these implementations.

In the present paper, we adopt new parameterisations of star formation and of the suppression of cooling flows by central galaxy AGN activity, as introduced by Croton et al. (2005). In the following, we briefly summarise the main characteristics of these physical prescriptions where they differ from those used in our previous work.

Following Kauffmann (1996a) and Croton et al. (2005), we assume that the star formation occurs with a rate given by:

$$\psi = \alpha(M_{\text{cold}} - M_{\text{crit}})/t_{\text{dyn}}, \quad (1)$$

where M_{cold} and $t_{\text{dyn}} = R_{\text{disc}}/V_{\text{vir}}$ are the cold gas mass and the dynamical time of the galaxy, respectively. The dimensionless parameter α regulates the efficiency of the conversion of gas into stars. Star formation is allowed to occur only

¹ The Virgo consortium (<http://www.virgo.dur.ac.uk/>) is an international collaboration of astronomers dedicated to large scale cosmological simulation.

if the gas surface density is larger than a critical value (that is used to obtain M_{crit} in Eq. 1) given by:

$$\Sigma_{\text{crit}} = 1.2 \times 10^7 \left(\frac{V_{\text{vir}}}{200 \text{ km s}^{-1}} \right) \left(\frac{R}{10 \text{ kpc}} \right)^{-1} M_{\odot} \text{ kpc}^{-2} \quad (2)$$

Note that in De Lucia et al. (2004b) we did not assume a surface density threshold for the star formation but we assumed a dependence of the star formation efficiency on the circular velocity of the parent galaxy. This assumption was responsible for delaying the star formation in small haloes until lower redshifts, which correctly reproduces the observed trend for increasing gas fraction at lower luminosities. As explained in Kauffmann (1996a), the introduction of a surface density threshold also naturally reproduces the observed trend of the gas fraction as a function of galaxy luminosity, due to the fact that the gas density always remains close to the critical gas surface density value. We postpone a more detailed investigation on how the census of ages and metallicities is influenced by the assumptions on the star formation and feedback model to a forthcoming paper. With respect to the trends presented in this paper, we have verified that the two different assumptions produce very similar results.

As in De Lucia et al. (2004b), we assume that bulge formation takes place during mergers: in the case of a ‘minor’ merger, we transfer the stellar mass of the merged galaxy to the bulge of the central galaxy and update the photometric properties of this galaxy. The cold gas of the satellite galaxy is added to the disk of the central galaxy and a fraction of the combined cold gas from both galaxies is turned into stars as a result of the merger. Any stars that formed during the burst are also added to the disk of the central galaxy. If the mass ratio of the merging galaxies is larger than 0.3, we assume that we witness a ‘major’ merger that gives rise to a more significant starburst and destroys the disk of the central galaxy completely, producing a purely spheroidal stellar distribution. Note that the galaxy can grow a new disc later on, provided it is fed by an appreciable cooling flow. Our starburst implementation is based on the ‘collisional starburst’ model introduced by Somerville et al. (2001) (see Croton et al. (2005) for details).

Following Croton et al. (2005), we extend the spheroid formation by assuming that bulges can also grow from disk instabilities, based on the the analytic model for disk formation by Mo, Mao & White (1998). We note that the addition of this channel for bulge formation does not substantially modify the trends presented in this paper. However, this additional physical mechanism changes the relative fractions of different morphological types. For the model explored in this paper, the final fractions of ellipticals, spirals, and lenticulars brighter than -18 in the V-band are 17, 65, and 18 per cent, respectively, and are very close to the observed relative fractions 13, 67, and 20 per cent measured by Loveday (1996). If bulge growth through disk instabilities is switched off, the above fractions become: 7, 84, and 8 per cent respectively. Considering only galaxies brighter than -20 , the fractions cited above become: 23, 58, and 19 for our default model and 13, 67, and 20 for a model where bulge growth through accretion is switched off. These numbers suggest that this channel of bulge formation may be more important for fainter ellipticals. We will come back to this issue in Sec. 5.

As in previous work, we determine the morphology of our model galaxies by using the B-band bulge-to-disc ratio together with the observational relation by Simien & de Vaucouleurs (1986) between this quantity and the galaxy morphological type. For the numbers quoted above and for the following analysis, we classify as ellipticals all galaxies with $\Delta M < 0.4$ ($\Delta M = M_{\text{bulge}} - M_{\text{total}}$), as spirals or irregulars all galaxies with $\Delta M > 1.56$, and as lenticulars (S0) all galaxies with intermediate value of ΔM . We include in our analysis all galaxies with stellar mass larger than $3 \times 10^8 M_{\odot}$. Note that, although we are essentially complete down to this mass limit, the less massive galaxies included in this analysis reside in substructures whose mass accretion history can be followed back in time in many cases only for a small number of snapshots. The determination of the morphological type then becomes quite noisy and uncertain. We estimate that our morphological type determination is robust for galaxies with mass equal to a few times $10^9 M_{\odot}$. The inclusion of galaxies below this limit, however, does not affect our main results of this study. When necessary, we will explicitly show results including only galaxies with mass larger than $4 \times 10^9 M_{\odot}$, whose morphological type can be considered ‘secure’. Our final sample contains 1,031,049 elliptical galaxies with stellar mass larger than $4 \times 10^9 M_{\odot}$. 810,486 of these have stellar mass larger than $1 \times 10^{10} M_{\odot}$.

Finally, we use the model of Croton et al. (2005) to describe central heating by AGN in massive groups and clusters and the associated suppression of cooling flows. In this model, gas condensation in massive systems is efficiently suppressed by ‘radio mode’ outflows that occur when a massive black hole finds itself at the centre of a static hot gas halo. The importance of these outflows grows with decreasing redshift and with the mass of the system. We refer to the original paper for full details and the physical motivation for this feedback implementation. We will later discuss in more detail the effect that this particular implementation has on the trends presented in our study.

4 THE STAR FORMATION HISTORY OF ELLIPTICAL GALAXIES

As discussed earlier, the uniformly red and old stellar populations of elliptical galaxies have traditionally been interpreted as evidence for a formation scenario in which these galaxies form in a single intense burst of star formation at high redshift and then passively evolve to the present day. Direct observations of the formation and evolution of early type galaxies are, however, difficult, and are plagued by the so called ‘progenitor-bias’ (van Dokkum & Franx 1996). One approach that is adopted to constrain the formation mechanism of these galaxies is that of studying in detail their stellar populations by means of population synthesis techniques. This method has its roots in a pioneering study by Tinsley (1972), and has become increasingly popular after the introduction of more detailed population synthesis models (Bruzual A. 1983; Guiderdoni & Rocca-Volmerange 1987; Buzzoni 1989). Recent improvements have come through the development of medium to high resolution spectral models that include quite complete libraries of stellar spectra and improved treatments of stellar evolu-

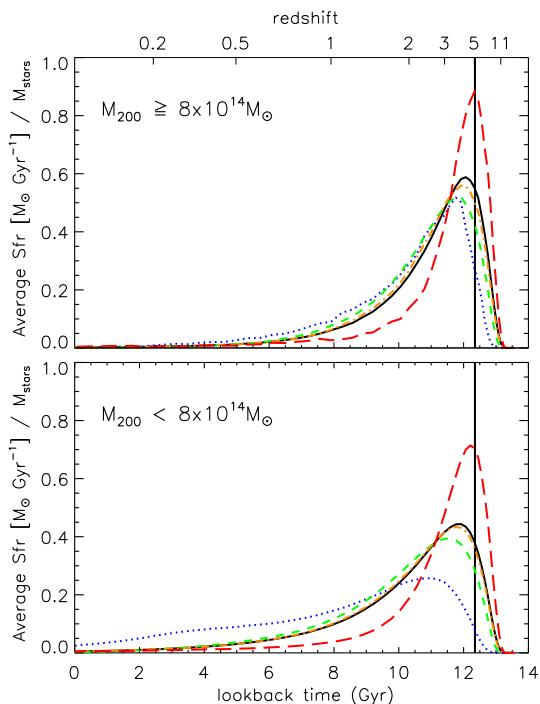


Figure 1. Average star formation histories of model elliptical galaxies split into bins of different stellar mass, normalised to the total mass of stars formed. The two panels are for galaxies residing in haloes of different mass, as indicated by the labels. In both panels, the solid line shows the average star formation history for all the elliptical galaxies in the sample under investigation. The long dashed, dash-dotted, dashed, and dotted lines refer to galaxies with stellar mass $\simeq 10^{12}$, 10^{11} , 10^{10} , and $10^9 M_{\odot}$ respectively. The vertical line in both panels is included to guide the eye.

tionary theory (Vazdekis 2001; Bruzual & Charlot 2003; Thomas, Maraston & Bender 2003).

The use of these more sophisticated models, together with the acquisition of better and larger amounts of data have recently established firm evidence for a mass-dependent evolutionary history of the elliptical galaxy population (De Lucia et al. 2004c; Kodama et al. 2004; Thomas et al. 2005; van der Wel et al. 2005; Treu et al. 2005). The data suggest that less massive ellipticals have more extended star formation histories than their more massive counterparts, giving them a *lower* characteristic *formation redshift*, in marked contrast to naive expectations based on the growth of dark matter halos in hierarchical CDM cosmologies. This observational finding is compatible with the “down-sizing” scenario for star formation proposed earlier (Faber et al. 1995; Cowie et al. 1996).

In this section, we study in detail the star formation histories of model elliptical galaxies and their dependence on stellar mass and environment. In Fig. 1, we show the average star formation history, normalised to the total mass of stars formed, for model elliptical galaxies split into different bins of stellar mass. The two panels are for galaxies residing in haloes of different mass. In the following we will refer to galaxies in haloes with mass $\gtrsim 8 \times 10^{14} M_{\odot}$ as ‘cluster’ ellipticals and as ‘field’ ellipticals to all model ellipticals residing in less massive haloes. In both panels, the solid line

shows the average star formation history for all the elliptical galaxies in the sample under investigation. The long dashed, dash-dotted, dashed, and dotted lines refer to galaxies with stellar mass $\simeq 1 \times 10^{12}$, 1×10^{11} , 1×10^{10} , and $1 \times 10^9 M_{\odot}$, respectively². The vertical lines are included to guide the eye and mark the peak of the $10^{12} M_{\odot}$ -ellipticals in the top panel.

Fig. 1 shows the most important result of this paper: more massive elliptical galaxies have star formation histories that peak at higher redshifts ($\simeq 5$) than lower mass systems, and can reach star formation rates up to several thousands of solar masses per year for galaxies ending up in overdense regions. Less massive elliptical galaxies have star formation histories that peak at progressively lower redshifts and are extended over a longer time interval.

A comparison of the top and bottom panels of Fig. 1 shows that the qualitative behaviour for ‘field’ and ‘cluster’ ellipticals is the same, but that for fixed mass, the star formation histories of field ellipticals are predicted to be more extended than those of ellipticals in clusters. This is a natural outcome of the hierarchical scenario, where haloes in regions of the Universe that are destined to form a cluster collapse earlier and merge more rapidly. The star formation histories shown in Fig. 1 represent averages computed over all the elliptical galaxies in the simulation box, but the trends remain true also when a much smaller volume of the simulation, and hence a much smaller sample size, is analysed. Fig. 2 shows the star formation histories of randomly selected elliptical galaxies in different mass bins and in different environments. The figure shows that individual star formation histories display a much more ‘bursty’ behaviour than those shown in Fig. 1. This reflects our assumption that bulge formation takes place during merger-induced bursts, which naturally gives the star formation histories of individual systems a bursty nature quite different from the smooth history seen for the population average. We will comment more on the implications of this for the scatter of the ages for the model elliptical galaxies in the following section.

In Fig. 3, we show the star formation histories again, but this time split into bins of different parent *halo mass*. The long dashed, dash-dotted, dashed, and dotted lines are for elliptical galaxies in haloes of mass $\simeq 1 \times 10^{15}$, 1×10^{14} , 1×10^{13} , and $1 \times 10^{12} M_{\odot}$ respectively³. Only galaxies with stellar mass larger than $4 \times 10^9 M_{\odot}$ are used here. The solid line shows the average mass-weighted star formation history for all the galaxies in the sample. The faster evolution of proto-cluster regions produces star formation histories that peak at higher redshifts for galaxies in more massive haloes. Given that galaxies of a fixed stellar mass occur in haloes covering a wide range of masses, it is not surprising that the dependence of the star formation history on halo mass is much weaker than that on galaxy stellar mass.

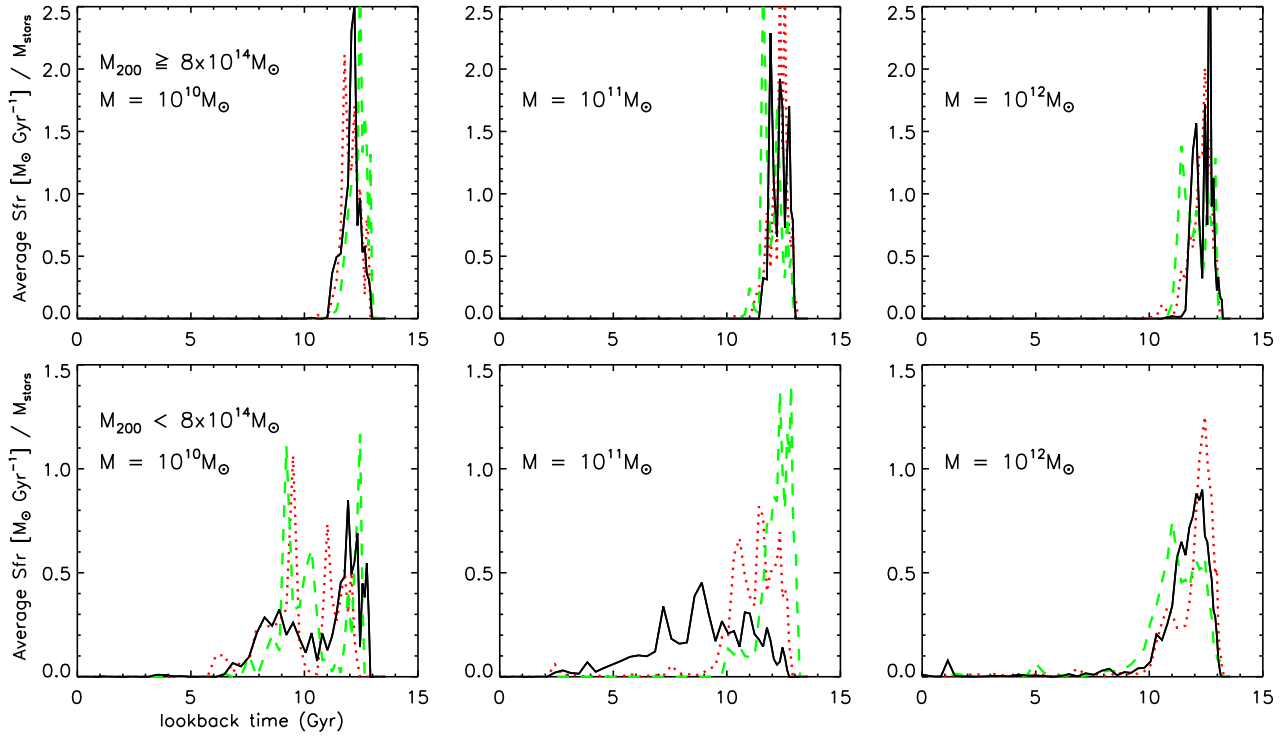


Figure 2. Each panel shows the star formation history for three randomly selected model elliptical galaxies in the given mass bin.

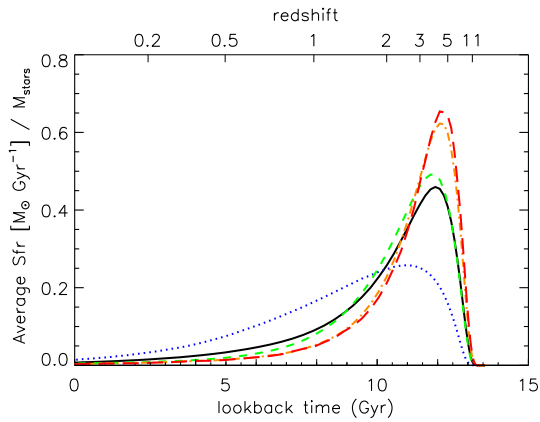


Figure 3. As in Fig. 1, but with model elliptical galaxies split into bins of different *parent halo mass*. The solid line shows the average mass-weighted star formation history for all the elliptical galaxies in the sample under investigation. The long dashed, dash-dotted, dashed, and dotted lines refer to galaxies residing in haloes with mass $M_{200} \simeq 10^{15}$, 10^{14} , 10^{13} , and $10^{12} M_{\odot}$, respectively.

5 THE DISTRIBUTION OF AGES AND METALLICITY

We now turn to an analysis of the distribution of ages and metallicities of model elliptical galaxies as a function of stellar mass and environment. In Fig. 4, we show the distribution of the formation redshifts for model elliptical galaxies. We define the formation redshift as the redshift when 50 per cent (or 80 per cent) of the stars that make up the final elliptical galaxy at redshift zero are already formed. The shaded histograms are for model elliptical galaxies with stellar mass larger than $10^{11} M_{\odot}$, while the open histogram is for all galaxies with secure morphology (stellar mass larger than $4 \times 10^9 M_{\odot}$). The figure clearly demonstrates that the stars in more massive ellipticals are on average older than those in their less massive counterparts, but the scatter of the distribution is rather large and there is a non-negligible fraction of model galaxies whose stars are formed relatively late.

It is important, however, to distinguish the early *formation times* of the stars that make up the elliptical galaxy population (reflected in the ‘down-sizing’ scenario) from the *assembly time* of the more massive ellipticals. If massive ellipticals form a large fraction of their stars in a number of distinct progenitor systems before they coalesce, these two times may well be quite different. Fig. 5 demonstrates that

² The actual bin size used for Figs. 1 and 2 is $7 \times 10^x M_{\odot} < M_{\text{stars}} < 2 \times 10^{x+1} M_{\odot}$, with $x = 8, 9, 10$, and 11 .

³ The actual bin size used is $7 \times 10^x M_{\odot} < M_{200} < 2 \times 10^{x+1} M_{\odot}$, with $x = 11, 12, 13$, and 14 .

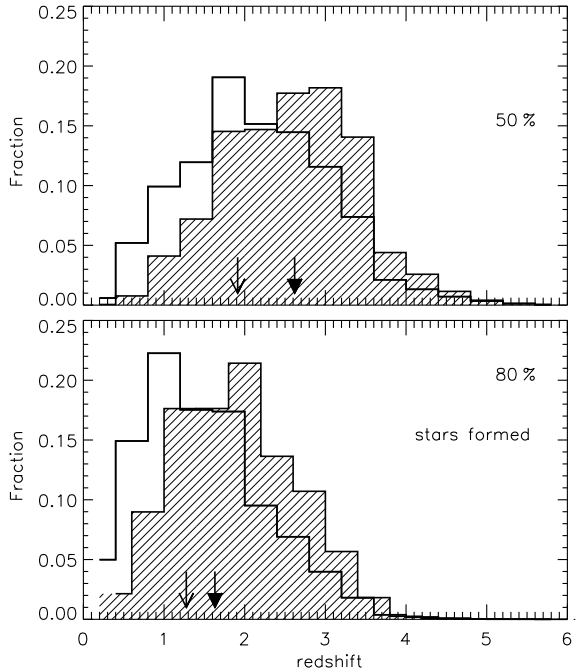


Figure 4. Distribution of the formation redshifts of model elliptical galaxies. In the upper (lower) panel, the formation redshift is defined as the redshift when 50 per cent (80 per cent) of the stars that make up the elliptical galaxy at redshift $z = 0$ are already formed. The shaded histogram is for elliptical galaxies with stellar mass larger than $10^{11} M_{\odot}$, while the open histogram is for all the galaxies with mass larger than $4 \times 10^9 M_{\odot}$. Arrows indicate the medians of the distributions, with the thick arrows referring to the shaded histograms. Note that more massive ellipticals typically form their stars earlier.

this is indeed the case in our model. We here show the distribution of the assembly redshifts for the same galaxies that we analysed in Fig. 4. We define the assembly time as the redshift when 50 per cent (or 80 per cent) of the final stellar mass is already contained in a single object. For galaxies more massive than $10^{11} M_{\odot}$, the median redshift when half of the stars are formed is ~ 2.5 (upper panel of Fig. 4), but for the same galaxies, half of their stars are typically assembled in a single object only at redshift ~ 0.8 (upper panel of Fig. 5). In addition, more massive galaxies assemble later than less massive ones, and only about half of the model elliptical galaxies have a progenitor with mass at least equal to half of their final mass at redshifts $\gtrsim 1.5$. The assembly history of ellipticals hence parallels the hierarchical growth of dark matter halos, in contrast to the formation history of the stars themselves. Note that the ‘gap’ between assembly redshifts and formation redshifts for the stars grows towards more massive ellipticals. Figs. 4 and 5 imply that a significant fraction of present elliptical galaxies has assembled relatively recently through purely stellar mergers. This finding agrees with recent observational results (van Dokkum 2005; Faber et al. 2005; Tran et al. 2005; Bell et al. 2005).

Table 1 lists, for different mass bins, medians and upper and lower quartiles of the distributions of lookback times

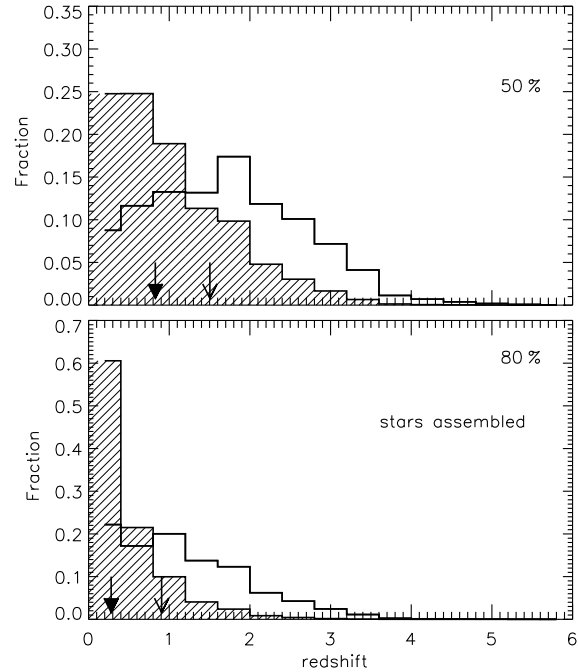


Figure 5. As in Fig. 4, but for the assembly redshifts of model elliptical galaxies. We define the assembly redshift as the time when 50 per cent (80 per cent) of the stars that make up the galaxy at redshift zero are already assembled in one single object. Note that more massive ellipticals typically assemble their stars later (cf Fig. 4).

corresponding to the formation and assembly redshifts defined above.

The large volume of our simulation allows us to study how properties of model elliptical galaxies depend on their stellar mass and on the environment. Fig. 6 shows how the luminosity-weighted age (panel a), the metallicity of the stellar component (panel b), and the B–V colour (panel c), depend on the galaxy stellar mass. In each panel, filled circles represent the median of the distributions, while the error bars mark the upper and lower quartiles. In the upper panel, the empty circles show the lookback times corresponding to the formation redshifts as defined in the upper panel of Fig. 4. The ages of model elliptical galaxies range from $\simeq 4$ Gyr for galaxies with mass a few times larger than $10^8 M_{\odot}$ to $\simeq 10$ Gyr for galaxies with mass $\simeq 10^{12} M_{\odot}$. It is interesting to note that the lookback time corresponding to the redshift when half of the stars had formed is a very good approximation to the luminosity-weighted age over the full range of masses shown. The age of model elliptical galaxies also seems to flatten at stellar masses $\simeq 10^{10} M_{\odot}$. The same flattening is observed for the B–V colour and, although weaker, for the stellar metallicity. Note that the scatter in these quantities (particularly for the colour and metallicity) is very small, indicating that the main driver of these trends is the stellar mass, as also reflected in Fig. 1. We note in passing that our model elliptical galaxies follow a colour-magnitude relation that is well defined up to $z \simeq 1$.

Table 1. Formation times and assembly times for model elliptical galaxies in different mass bins. The first two columns indicate the extrema of the mass bins. The next columns list the lower quartile, the median, and upper quartile for each of the formation and assembly times defined in the text. Tf50, Tf80 represent the lookback times corresponding to the redshifts when 50 or 80 per cent of the stars were first formed. Ta50 and Ta80 represent the lookback times corresponding to the redshifts when 50 or 80 per cent of the mass was first assembled in a single object. All times are in Gyr. Masses are in units of M_{\odot} .

M_{low}	M_{up}	Tf50			Tf80			Ta50			Ta80		
2.5×10^9	1.25×10^{10}	8.90	10.06	11.01	6.84	8.58	10.06	8.25	9.78	10.79	6.10	8.25	9.78
1.25×10^{10}	6.25×10^{10}	9.20	10.31	11.01	7.20	8.90	10.06	7.91	9.78	10.56	5.35	7.91	9.50
6.25×10^{10}	3.12×10^{11}	9.78	10.56	11.22	7.56	9.20	10.31	4.97	7.91	9.78	1.76	4.22	7.20
3.12×10^{11}	1.56×10^{12}	11.01	11.41	11.76	9.50	10.31	10.79	3.13	4.97	6.84	0.83	2.09	3.85

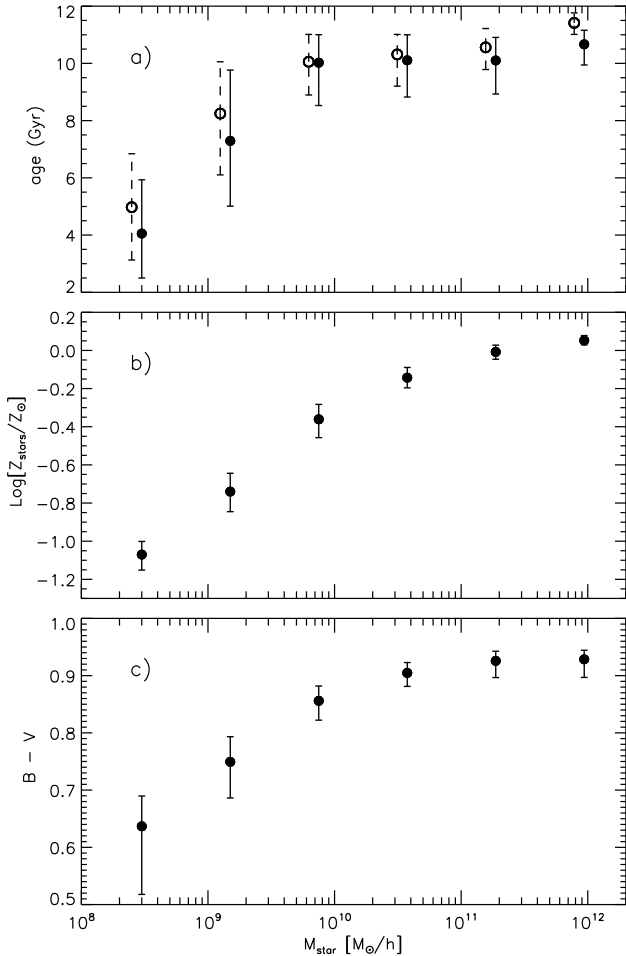


Figure 6. Median luminosity-weighted age (panel a), stellar metallicity (panel b), and $B-V$ colour (panel c) of model elliptical galaxies as a function of their stellar mass. Symbols indicate the median value of the distributions at each mass, while the error bars link the upper and lower quartiles. The open symbols in the top panel correspond to the lookback time of the upper panel in Fig. 4.

The results shown in Fig. 6 also indicate that this relation is mainly driven by metallicity, in line with the common interpretation of the evolution of the slope and the zero-point of the observed relation as a function of redshift. We plan to investigate the relative contribution of age and metallicity in

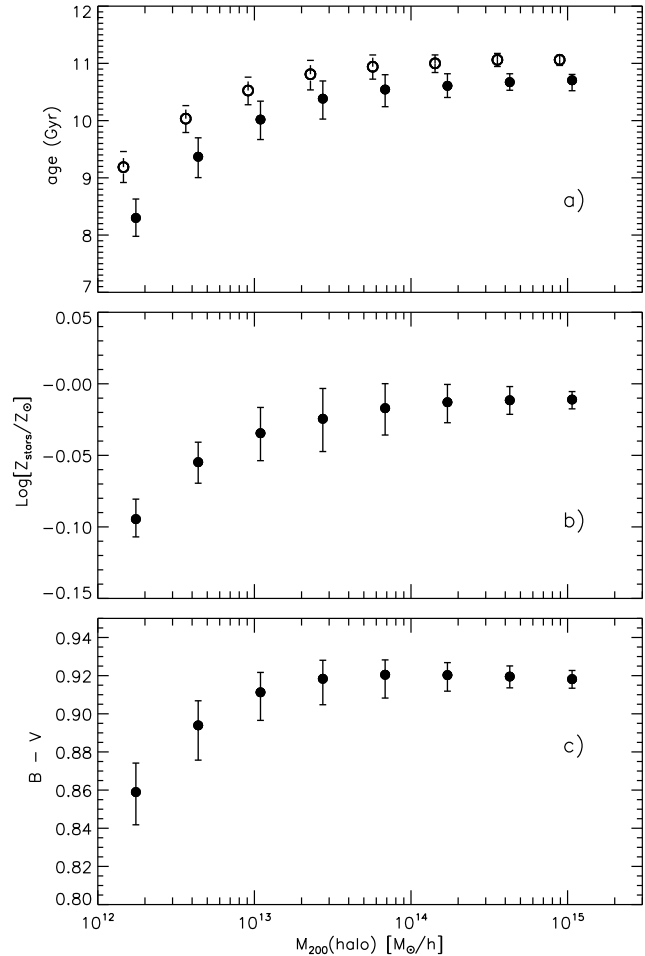


Figure 7. The same quantities as in Fig. 6, but now calculated as mass-weighted average over all galaxies in a halo and shown as a function of the virial mass of the halo. Only elliptical galaxies with stellar mass larger than $4 \times 10^9 M_{\odot}$ are included here.

shaping the observed colour-magnitude relation in a future paper.

In Fig. 7 we show the same quantities as in Fig. 6 but as a function of the virial mass of the halo in which the galaxies reside. Only galaxies with stellar mass larger than $4 \times 10^9 M_{\odot}$ are included here. For each halo, we compute the mass-weighted average age, metallicity and colour. Fig. 7 shows the median of these values and the upper and lower

quartiles of the distribution. Elliptical galaxies in high density environments are on average older, more metal rich, and redder than isolated elliptical galaxies. Elliptical galaxies in clusters form a homogeneously old population and elliptical galaxies in groups (haloes with mass $\simeq 10^{13} M_{\odot}$) are as old as or slightly younger than galaxies in massive clusters (haloes with mass $\simeq 10^{15} M_{\odot}$), while elliptical galaxies in smaller groups exhibit a lower median age. This is in agreement with recent observational results (Terlevich & Forbes 2002; Proctor et al. 2004). The median stellar metallicities of galaxies in our clusters are higher than the corresponding values for the field. Elliptical galaxies in these systems show a remarkably small spread in colour with a median $B-V$ colour that is almost independent of environment down to the mass-scale $\simeq 10^{13} M_{\odot}$ of groups.

We can also investigate how the properties of model elliptical galaxies depend on cluster-centric distance. This is shown in Fig. 8, based on all elliptical galaxies in haloes with $M_{200} \gtrsim 8 \times 10^{14} M_{\odot}$ and with stellar mass larger than $4 \times 10^9 M_{\odot}$. We find in total 51 clusters in the whole simulation box with virial mass larger than this value. Fig. 8 shows that galaxies closer to the centre are on average older and more metal rich than galaxies at the outskirts of these clusters. The bottom panel of Fig. 8 shows that this trend is partly driven by mass segregation. A radial dependence of galaxy properties is, however, also a natural consequence of the fact that mixing of the galaxy population is incomplete during cluster assembly. This implies that the cluster-centric distance of the galaxies is correlated with the time they were accreted onto a larger structure (Diaferio et al. 2001; Gao et al. 2004). The values of the median age, metallicity, and colour all flatten at distance $\simeq R_{200}$. The scatter shown in Fig. 8 is rather large but in the very centre of the clusters, where elliptical galaxies are all very old ($\simeq 12$ Gyr), they have about solar metallicity, and have very red $B-V$ colour ($\simeq 0.95$).

In the hierarchical galaxy formation scenario, elliptical galaxies form through mergers of smaller units, and larger systems are expected to be made up by a larger number of progenitor galaxies. A very interesting question is therefore how large the number of progenitor systems of galaxies is, and how this number varies as a function of final mass. To get a quantitative handle on this question, we define for each galaxy an *effective number of stellar progenitors* by computing the quantity

$$N_{\text{eff}} = \frac{M_{\text{final}}^2}{2 \sum_i m_i M_{i,\text{form}}}, \quad (3)$$

where m_i denotes the masses of all the stars that make up a galaxy of final mass $M_{\text{final}} = \sum_i m_i$. The quantity $M_{i,\text{form}}$ gives the stellar mass of the galaxy within which the star i formed, at the time of formation of the star. In the case where all stars form in a single object that grows to the final stellar mass without experiencing any merger, Eq. (3) can be viewed as a discretised form of the integral

$$N_{\text{eff}} = \frac{M_{\text{final}}^2}{\int_0^{M_{\text{final}}} 2 M dM},$$

which evaluates to $N_{\text{eff}} = 1$ independent of the detailed star formation history. However, if a galaxy is assembled from several pieces we expect a larger value of N_{eff} , because then the values of $M_{i,\text{form}}$ that enter the sum in the denomina-

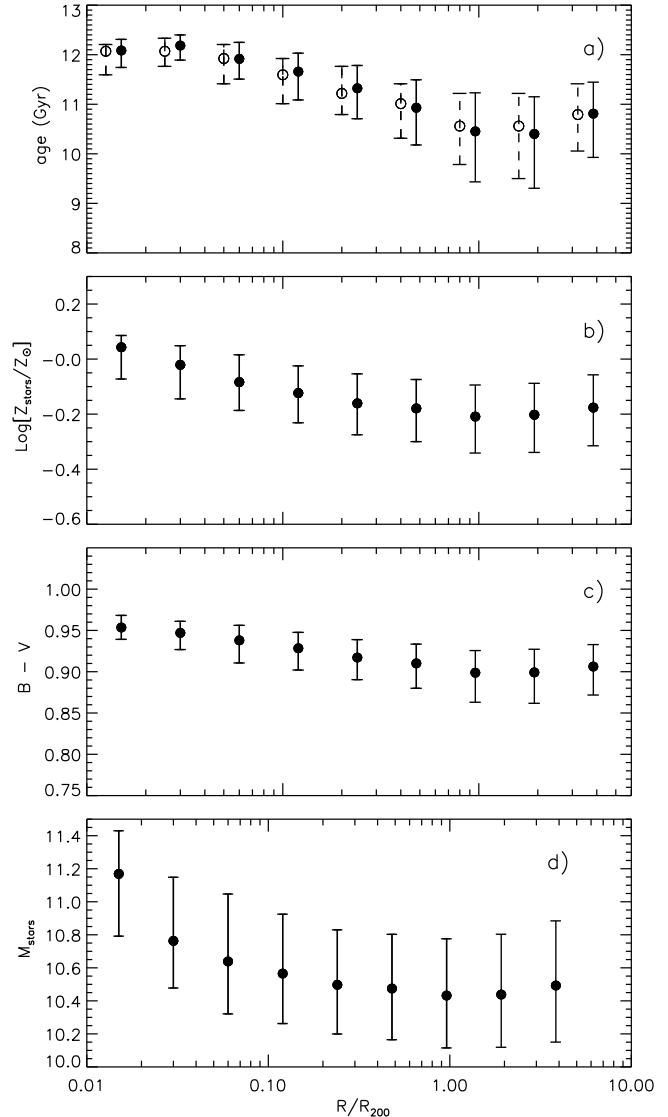


Figure 8. Median luminosity-weighted age (panel a), stellar metallicity (panel b), $B-V$ colour (panel c), and stellar mass (panel d) for model elliptical galaxies in dark matter haloes with mass $\gtrsim 8 \times 10^{14} M_{\odot}$ as a function of the distance from the cluster centre. Symbols and lines have the same meaning as in Fig. 6.

tor of Eq. (3) become lower. For example, if the stars of a galaxy were formed in two progenitors of equal final size, which then merged into a single object without any further star formation, we obtain $N_{\text{eff}} = 2$. Note that in more general cases we will obtain fractional values for N_{eff} due to the mass-weighting of the progenitors, which is built into the definition of N_{eff} . For example, if a galaxy is made up of three pieces that contain one half, one quarter and one quarter of the final stellar mass, respectively, one gets $N_{\text{eff}} = 8/3$, which is less than the absolute number of progenitors. This reflects the fact that the majority of the stars formed in a single object. The mass-weighting hence delivers an effective count of the progenitors by giving weight only to those progenitor systems that contribute significantly to the final

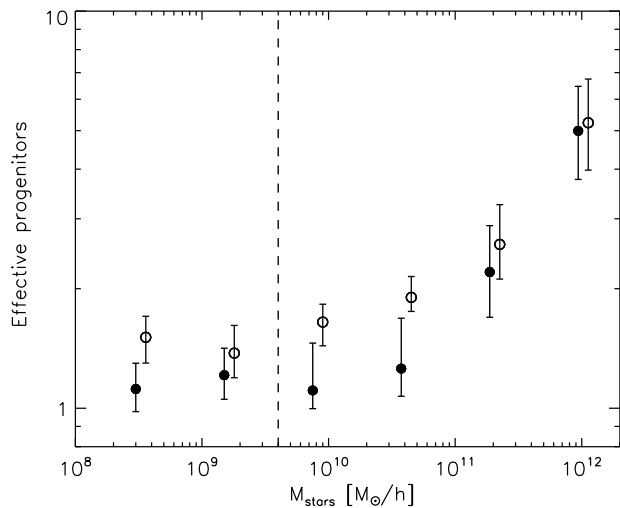


Figure 9. Effective number N_{eff} of progenitors as a function of galaxy stellar mass. Filled circles represent the median of the distribution in our default model, while the error bars indicate the upper and lower quartiles. Empty circles and the corresponding error bars are for a model where bulge formation through disk instability is switched off. The vertical dashed line corresponds to the limit above which our morphological type determination is robust (see Sec. 3).

stellar mass of the galaxy. In contrast, a count of the total number of progenitors would be dominated by the large number of negligibly small satellites that fall into a galaxy during its growth in a hierarchical universe. We therefore argue that N_{eff} is a more useful proxy for the number of significant mergers required to assemble a galaxy. We caution however that a straightforward interpretation of N_{eff} in the context of spheroid formation is complicated by the fact that bulges can also grow in our model without mergers, through disk instabilities.

In Fig. 9, we show the effective number of progenitors as a function of galaxy stellar mass. Filled circles represent the median of the distributions in our default model while empty circles represent the median of the distributions in a model where bulge growth through disk instability is switched off. Interestingly, bulge growth through disk instability seems to be an efficient process for intermediate mass ellipticals but rather ineffective for the most massive ellipticals in our sample. As expected, more massive galaxies are made up of more pieces. Fig. 9 shows that the number of effective progenitors is less than 2 up to stellar masses of $\approx 10^{11} M_{\odot}$, indicating that the formation of these systems typically involves only a small number of major mergers. Only galaxies more massive than $\approx 10^{11} M_{\odot}$ are built up through a larger number of mergers, reaching up to $N_{\text{eff}} \approx 5$ for the most massive galaxies. We recall that these most massive elliptical galaxies are, however, also the ones with the oldest stellar populations. We note that the monolithic collapse scenario would predict $N_{\text{eff}} = 1$ for these large ellipticals, in marked difference to our hierarchical prediction.

6 DISCUSSION AND CONCLUSIONS

We have combined a large high-resolution cosmological N -body simulation with semi-analytic techniques to investigate the formation and evolution of elliptical galaxies in a hierarchical merger model. Understanding the formation and the evolution of these systems represents an issue of fundamental interest as 50 per cent or more of the stellar mass in the local Universe appears to be in early-type systems and bulges (Bell et al. 2003).

In this paper, we have focused on the dependence of the star formation histories, ages, and metallicities on environment and on galaxy stellar mass. In our model, we find that elliptical galaxies in denser environments are on average older, more metal rich, and redder than the general population of ‘field’ ellipticals. This can be attributed to the fact that high density regions form from the highest density peaks in the primordial field of density fluctuations, whose evolution is somewhat accelerated with respect to regions of ‘average’ density. There is also a clear trend for increasing ages and metallicities, and for redder colours, with decreasing cluster-centric distance. This can again be viewed as a natural expectation of hierarchical models where the distance of the galaxies from the cluster centre is correlated with the time they were accreted onto the larger system. When this infall happens, we assume that the galaxy is stripped of its hot gas reservoir so it is no longer able to accrete fresh material for star formation. The galaxy then rapidly consumes its cold gas moving towards the red sequence.

We have also investigated how the properties of model elliptical galaxies change as a function of the stellar mass. We have shown – and this is perhaps the most important result of our study – that in our model the most massive elliptical galaxies have the oldest and most metal rich stellar populations, in agreement with observational results (see for example Nelan et al. 2005). In addition, they are also characterised by the shortest formation time-scales, in qualitative agreement with the recently established down-sizing scenario (Cowie et al. 1996). However, these old ages are in marked contrast to the late assembly times we find for these galaxies. In fact, our results show that massive ellipticals are predicted to be assembled *later* than their lower mass counterparts, and that they have a larger effective number of progenitor systems. This is a key difference between the hierarchical scenario and the traditional monolithic collapse picture.

Our results disagree with previous semi-analytic models that found a trend for more massive ellipticals to be *younger* than less massive ones (Kauffmann 1996b; Baugh et al. 1996; Kauffmann & Charlot 1998). In order to understand the origin of this discrepancy we have re-run our model with different assumptions. Fig. 10 shows the average star formation histories of all model elliptical galaxies split into bins of different stellar mass and normalised to the total mass of stars formed, as in Fig. 1. In the upper panel, we repeat the results obtained for the ‘standard’ model used in our analysis, which employs the suppression of cooling flows by central AGN activity as introduced by Croton et al. (2005). In the middle panel, we show the same results but for a model in which no AGN feedback and no artificial cooling cutoff is included. Finally, in the bottom panel, we show results ob-

tained for a model in which galaxy cooling is switched off in haloes with $V_{\text{vir}} > 350 \text{ km s}^{-1}$ - the *ad hoc* suppression used in many previous models, including those of De Lucia et al. (2004b).

Fig. 10 clearly shows that when no suppression of the condensation of gas in massive haloes is considered, the most massive ellipticals have the most extended star formation histories. Too many massive systems are, however, produced at redshift zero, at odds with observations. Late mergers and late accretion, which still involve a substantial amount of gas in this model, cause the formation of luminous and young bulge stars. An artificial cutoff of the gas condensation, similar to that employed in previous models, produces results that are qualitatively similar (see also De Lucia 2004) to those obtained with the more physically motivated AGN model introduced by Croton et al. (2005), as is shown in the bottom panel of Fig. 10. The figure also indicates however, that the model does not produce a monotonic behaviour as a function of stellar mass.

This is better seen in Fig. 11 where we show the median luminosity-weighted ages of model elliptical galaxies as a function of their stellar mass for the same three models. Filled circles show the result for the model with AGN feedback, open circles show the result for the model without AGN feedback and without any artificial cutoff, and filled triangles show the result for the model with the artificial cooling cutoff. The lines coincide perfectly up to stellar masses $\simeq 5 \times 10^{10} M_{\odot}$. For larger masses, the median age stays almost constant for the model with AGN feedback, decreases for the model without suppression of the cooling flows, and shows a non-monotonic behaviour for the model with an artificial cooling cutoff. We note, however, that the differences between this scheme and a model with AGN feedback are small. In our analysis, a cooling flow cut-off is hence able to approximately produce the same result as AGN feedback, which is still different from many earlier results.

We note that the earlier semi-analytic results were based on Monte-Carlo merger trees constructed with the extended Press-Schechter formalism, and not by measuring merger trees directly from high-resolution numerical simulations as we have done here. Although there have been suggestions that the extended Press-Schechter theory may not provide a sufficiently accurate description of the merger trees (Benson, Kamionkowski & Hassani 2005), it seems unlikely that this is responsible for reversing the trends found in this analysis. We believe this reversal to be a combination of the change in the physical model and in the cosmology. We note that the work of Kauffmann & Charlot (1998) was carried out in the framework of a cosmological model with critical matter density, where massive haloes are formed much later than in a low-density Universe normalised to the same cluster abundance. In addition, Kauffmann & Charlot (1998) employed an artificial cooling cutoff corresponding to a critical velocity equal to 500 km s^{-1} . This leaves room for late gaseous mergers and gas accretion that can substantially rejuvenate the stellar population of elliptical galaxies.

Another important difference between our model and previous ones is that we explicitly follow dark matter substructures within each halo, even after their progenitor halos have been accreted by larger structures. Springel et al. (2001) have shown that this allows a more faithful tracking of the orbits of galaxies and an improved modelling of the

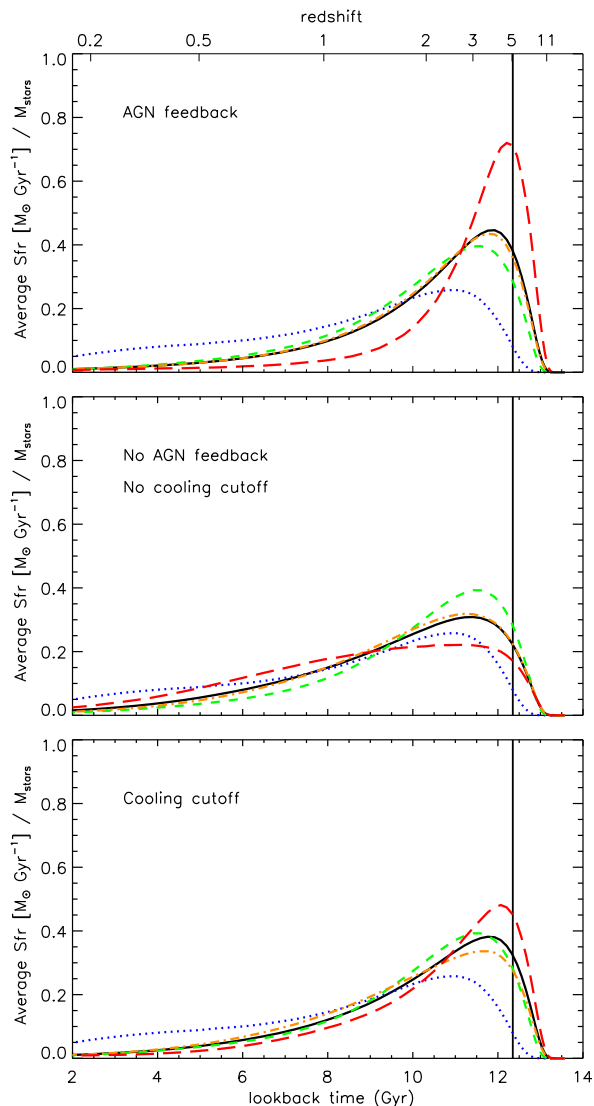


Figure 10. Average star formation histories of model elliptical galaxies split into bins of different stellar mass, normalised to the total mass of stars formed. In the upper panel, results are shown for the ‘standard’ model used for our analysis, which employs the suppression of cooling flows by central galaxy AGN activity, as introduced by Croton et al. (2005). In the middle panel, results are shown for a model without AGN feedback and without any cooling cutoff. Finally, in the bottom panel, results are shown for a model without AGN feedback but with a cooling cutoff with a critical velocity equal to 350 km s^{-1} . Different line styles have the same meaning as in Fig. 1.

actual merging rate in any given halo. Most of the galaxies we classify as ellipticals are indeed genuine ‘satellite’ galaxies with their own self-bound dark matter subhalo. If too many of these satellite galaxies are assumed to merge on too short a timescale, excessively bright and blue central galaxies result.

The short formation time-scales we find for very massive ellipticals are qualitatively in agreement with those required by Thomas et al. (2005) in order to reproduce the observed α -element enhancements. The detailed census of

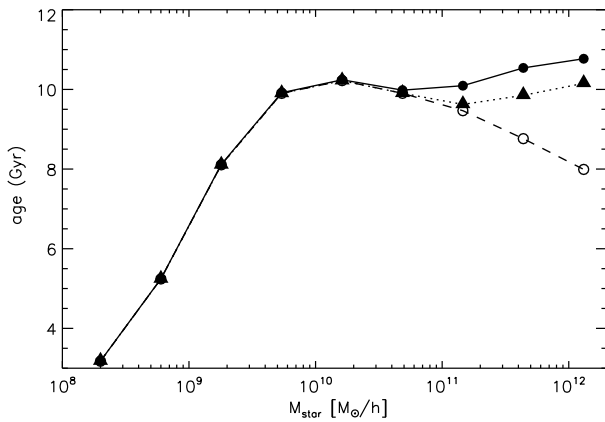


Figure 11. Median age of model elliptical galaxies as a function of galaxy stellar mass. Filled circles show results for our default model. Empty circles are for a model without AGN feedback and without any cooling cutoff. Filled triangles are for a model without AGN feedback but with a cooling cutoff with a critical velocity equal to 350 km s^{-1} .

ages and metallicities for stars in our model elliptical galaxies depends on details of our feedback model and chemical enrichment scheme. We plan to come back to these issues in future work.

Our results demonstrate that an apparent ‘down-sizing’ in the formation of ellipticals is not in contradiction with the hierarchical paradigm. Modern semi-analytic models of galaxy formation do predict ‘anti-hierarchical’ star formation histories for ellipticals in a Λ CDM universe even though the *assembly* of these galaxies is indeed hierarchical.

ACKNOWLEDGEMENTS

G. D. L. would like to thank M. Pannella and V. Strazzullo for intense and provocative discussions on our poor knowledge of galaxy formation and evolution. We thank B. Poggianti and A. Aragón-Salamanca for useful comments and stimulating discussions. G. D. L. thanks the Alexander von Humboldt Foundation, the Federal Ministry of Education and Research, and the Programme for Investment in the Future (ZIP) of the German Government for financial support.

This paper has been typeset from a $\text{T}_{\text{E}}\text{X}/\text{L}_{\text{A}}\text{T}_{\text{E}}\text{X}$ file prepared by the author.

REFERENCES

- Barger A. J., Aragon-Salamanca A., Ellis R. S., Couch W. J., Smail I., Sharples R. M., 1996, *MNRAS*, 279, 1
- Baugh C. M., Cole S., Frenk C. S., 1996, *MNRAS*, 283, 1361
- Bell E. F., McIntosh D. H., Katz N., Weinberg M. D., 2003, *ApJS*, 149, 289
- Bell E. F., Naab T., McIntosh D. H., Somerville R. S., Caldwell J. A. R., Barden M., Wolf C., Rix H.-W., Beckwith S. V. W., Borch A., Haeussler B., Heymans C., Jahnke K., Jogee S., Meisenheimer K., Peng C. Y., Sanchez S. F., Wisotzki L., 2005, *ApJ*, submitted, astro-ph/0506425
- Benson A. J., Kamionkowski M., Hassani S. H., 2005, *MNRAS*, 357, 847
- Bruzual G., Charlot S., 2003, *MNRAS*, 344, 1000
- Bruzual A. G., 1983, *ApJ*, 273, 105
- Buzzoni A., 1989, *ApJS*, 71, 817
- Colless M., Dalton G., Maddox S., Sutherland W., Norberg P., Cole S., Bland-Hawthorn J., Bridges T., et al., 2001, *MNRAS*, 328, 1039
- Cowie L. L., Songaila A., Hu E. M., Cohen J. G., 1996, *AJ*, 112, 839
- Croton D. J., Springel V., White S. D. M., De Lucia G., Frenk C. S., Gao L., Jenkins A., Kauffmann G., Navarro J. F., Yoshida N., 2005, *MNRAS*, in press, astro-ph/0508046
- De Lucia G., 2004, Ph.D. Thesis, Ludwig-Maximilian Universität, Munich
- De Lucia G., Kauffmann G., Springel V., White S. D. M., Lanzoni B., Stoehr F., Tormen G., Yoshida N., 2004, *MNRAS*, 348, 333
- De Lucia G., Kauffmann G., White S. D. M., 2004, *MNRAS*, 349, 1101
- De Lucia G., Poggianti B. M., Aragón-Salamanca A., Clowe D., Halliday C., Jablonka P., Milvang-Jensen B., Pelló R., Poirier S., Rudnick G., Saglia R., Simard L., White S. D. M., 2004, *ApJ*, 610, L77
- Denicoló G., Terlevich R., Terlevich E., Forbes D. A., Terlevich A., 2005, *MNRAS*, 358, 813
- Diaferio A., Kauffmann G., Balogh M. L., White S. D. M., Schade D., Ellingson E., 2001, *MNRAS*, 323, 999
- Faber S. M., Trager S., González J., Worthey G., 1995, in van der Kruit P. C., Gilmore G., eds, *Stellar Populations*. Kluwer, Dordrecht, p. 249
- Faber S. M., Willmer C. N. A., Wolf C., Koo D. C., Weiner B. J., Newman J. A., Im M., Coil A. L., et al., 2005, *ApJ*, submitted, astro-ph/0506044
- Farouki R. T., Shapiro S. L., 1982, *ApJ*, 259, 103
- Gao L., Springel V., White S. D. M., 2005, *MNRAS*, 363, L66
- Gao L., White S. D. M., Jenkins A., Stoehr F., Springel V., 2004, *MNRAS*, 355, 819
- Guiderdoni B., Rocca-Volmerange B., 1987, *A&A*, 186, 1
- Kauffmann G., 1995, *MNRAS*, 274, 161
- Kauffmann G., 1996a, *MNRAS*, 281, 475
- Kauffmann G., 1996b, *MNRAS*, 281, 487
- Kauffmann G., Charlot S., 1998, *MNRAS*, 294, 705
- Kauffmann G., Colberg J. M., Diaferio A., White S. D. M., 1999, *MNRAS*, 303, 188
- Kodama T., Arimoto N., Barger A. J., Aragón-Salamanca A., 1998, *A&A*, 334, 99
- Kodama T., Yamada T., Akiyama M., Aoki K., Doi M., Furusawa H., Fuse T., Imanishi M., et al., 2004, *MNRAS*, 350, 1005
- Larson R. B., 1975, *MNRAS*, 173, 671
- Loveday J., 1996, *MNRAS*, 278, 1025
- Mathis H., Lemson G., Springel V., Kauffmann G., White S. D. M., Eldar A., Dekel A., 2002, *MNRAS*, 333, 739
- Menanteau F., Abraham R. G., Ellis R. S., 2001, *MNRAS*, 322, 1
- Michard R., Prugniel P., 2004, *A&A*, 423, 833

- Mo H. J., Mao S., White S. D. M., 1998, MNRAS, 295, 319
- Negroponte J., White S. D. M., 1983, MNRAS, 205, 1009
- Nelan J. E., Smith R. J., Hudson M. J., Wegner G. A., Lucey J. R., Moore S. A. W., Quinney S. J., Suntzeff N. B., 2005, ApJ, 632, 137
- Partridge R. B., Peebles P. J. E., 1967, ApJ, 147, 868
- Proctor R. N., Forbes D. A., Hau G. K. T., Beasley M. A., De Silva G. M., Contreras R., Terlevich A. I., 2004, MNRAS, 349, 1381
- Schweizer F., Seitzer P., 1992, AJ, 104, 1039
- Simien F., de Vaucouleurs G., 1986, ApJ, 302, 564
- Somerville R. S., Primack J. R., Faber S. M., 2001, MNRAS, 320, 504
- Spergel D. N., Verde L., Peiris H. V., Komatsu E., Nolta M. R., Bennett C. L., Halpern M., Hinshaw G., Jarosik N., Kogut A., Limon M., Meyer S. S., Page L., Tucker G. S., Weiland J. L., Wollack E., Wright E. L., 2003, ApJS, 148, 175
- Springel V., White S. D. M., Jenkins A., Frenk C. S., Yoshida N., Gao L., Navarro J., Thacker R., Croton D., Helly J., Peacock J. A., Cole S., Thomas P., Couchman H., Evrard A., Colberg J., Pearce F., 2005, Nature, 435, 629
- Springel V., White S. D. M., Tormen G., Kauffmann G., 2001, MNRAS, 328, 726
- Terlevich A. I., Forbes D. A., 2002, MNRAS, 330, 547
- Thomas D., 1999, MNRAS, 306, 655
- Thomas D., Maraston C., Bender R., 2003, MNRAS, 339, 897
- Thomas D., Maraston C., Bender R., de Oliveira C. M., 2005, ApJ, 621, 673
- Tinsley B. M., 1972, A&A, 20, 383
- Toomre A., Toomre J., 1972, ApJ, 178, 623
- Tran K.-V. H., van Dokkum P., Franx M., Illingworth G. D., Kelson D. D., Schreiber N. M. F., 2005, ApJ, 627, L25
- Treu T., Ellis R. S., Liao T. X., van Dokkum P. G., 2005, ApJ, 622, L5
- Treu T., Stiavelli M., Casertano S., Møller P., Bertin G., 2002, ApJ, 564, L13
- van de Ven G., van Dokkum P. G., Franx M., 2003, MNRAS, 344, 924
- van der Wel A., Franx M., van Dokkum P. G., Rix H.-W., Illingworth G. D., Rosati P., 2005, ApJ, 631, 145
- van Dokkum P. G., 2005, AJ, in press, astro-ph/0506661
- van Dokkum P. G., Franx M., 1996, MNRAS, 281, 985
- van Dokkum P. G., Stanford S. A., 2003, ApJ, 585, 78
- Vazdekis A., 2001, Ap&SS, 276, 921
- Willis J. P., Hewett P. C., Warren S. J., Lewis G. F., 2002, MNRAS, 337, 953